1-1-2015

Study of the consequences of CO2 released from high-pressure pipelines

Xiong Liu
University of Wollongong, xiong@uow.edu.au

Ajit R. Godbole
University of Wollongong, agodbole@uow.edu.au

Cheng Lu
University of Wollongong, chenglu@uow.edu.au

Guillaume Michal
University of Wollongong, gmichal@uow.edu.au

Phillip Venton
Venton and Associates

Study of the consequences of CO2 released from high-pressure pipelines

Abstract

The development of the Carbon Capture and Storage (CCS) technique requires an understanding of the hazards posed by the operation of high-pressure CO_2 pipelines. To allow the appropriate safety precautions to be taken, a comprehensive understanding of the consequences of unplanned CO_2 releases is essential before the deployment of CO_2 pipelines. In this paper, we present models for the predictions of discharge rate, atmospheric expansion and dispersion due to accidental CO_2 releases from high-pressure pipelines. The GERG-2008 Equation of State (EOS) was used in the discharge and expansion models. This enabled more precise 'source strength' predictions. The performance of the discharge and dispersion models was validated against experimental data. Full-bore ruptures of pipelines carrying CO_2 mixtures were simulated using the proposed discharge model. The propagation of the decompression wave in the pipeline and its influence on the release rate are discussed. The effects of major impurities in the CO_2 mixture on the discharge rate were also investigated. Considering typical CO_2 mixtures in the CCS applications, consequence distances for CO_2 pipelines of various sizes at different stagnation pressures were obtained using the dispersion model. In addition, the impact of H2S in a CO_2 mixture was studied and the threshold value of the fraction of H_2S at the source for which the hazardous effects of H_2S become significant was obtained.

Keywords

co2, pressure, high, released, pipelines, study, consequences

Disciplines

Engineering | Science and Technology Studies

Publication Details

Liu, X., Godbole, A., Lu, C., Michal, G. & Venton, P. (2015). Study of the consequences of CO_2 released from high-pressure pipelines. Atmospheric Environment, 116 51-64.

Study of the consequences of CO_2 released from high-pressure pipelines

Xiong Liu[a], Ajit Godbole[a], Cheng Lu[a,*], Guillaume Michal[a], Philip Venton[b]

[a] School of Mechanical, Materials and Mechatronic Engineering, University of Wollongong, NSW 2522, Australia

[b] Venton and Associates Pty Ltd, Bundanoon, NSW 2578, Australia

Abstract

The development of the Carbon Capture and Storage (CCS) technique requires an understanding of the hazards posed by the operation of high-pressure CO_2 pipelines. To allow the appropriate safety precautions to be taken, a comprehensive understanding of the consequences of unplanned CO_2 releases is essential before the deployment of CO_2 pipelines. In this paper, we present models for the predictions of discharge rate, atmospheric expansion and dispersion due to accidental CO_2 releases from high-pressure pipelines. The GERG-2008 Equation of State (EOS) was used in the discharge and expansion models. This enabled more precise 'source strength' predictions. The performance of the discharge and dispersion models was validated against experimental data. Full-bore ruptures of pipelines carrying CO_2 mixtures were simulated using the proposed discharge model. The propagation of the decompression wave in the pipeline and its influence on the release rate are discussed. The effects of major impurities in the CO_2 mixture on the discharge rate were also investigated. Considering typical CO_2 mixtures in the CCS applications, consequence distances for CO_2 pipelines of various sizes at different stagnation pressures were obtained using the dispersion model. In addition, the impact of H_2S in a CO_2 mixture was studied and the threshold value of the fraction of H_2S at the source for which the hazardous effects of H_2S become significant was obtained.

Keywords: Carbon Capture and Storage; CO_2 pipeline; Equation of State; CO_2 dispersion; CFD modelling

* Corresponding author. Tel.: +61-2-4221-4639; Fax: +61-2-4221-5474.

E-mail address: chenglu@uow.edu.au (C. Lu).

Nomenclature			
A	area (m^2)	T_e	temperature at rupture exit (K)
A_a	area at ambient pressure plane (m^2)	u	velocity ($m\ s^{-1}$)
A_e	area at rupture exit (m^2)	u_a	velocity at ambient pressure plane ($m\ s^{-1}$)
C_s	roughness constant, dimensionless	u_e	velocity at rupture exit ($m\ s^{-1}$)
f_L	dense phase fraction, dimensionless	u_o	outflow velocity ($m\ s^{-1}$)
f_V	vapour phase fraction, dimensionless	u_r	reference wind velocity ($m\ s^{-1}$)
h	enthalpy ($J\ mol^{-1}$)	u_*	friction velocity ($m\ s^{-1}$)
h_a	enthalpy at ambient pressure plane ($J\ mol^{-1}$)	w	sonic speed ($m\ s^{-1}$)
h_e	molar enthalpy at rupture exit ($J\ mol^{-1}$)	w_0	sonic speed at stagnation conditions ($m\ s^{-1}$)
k	specific turbulent kinetic energy ($m^2\ s^{-2}$)	w_m	sonic speed of gas-liquid mixture ($m\ s^{-1}$)
K	von Karman constant, dimensionless	z	height above ground (m)
K_s	equivalent sand-grain roughness height (m)	z_0	surface roughness length (m)
L	Monin-Obukhov length (m)	z_r	reference height (m)
P	static pressure (Pa)		
P_0	stagnation pressure (Pa)	*Greek letters*	
P_a	ambient pressure (Pa)	α	wind shear exponent, dimensionless
P_e	pressure at rupture exit (Pa)	ε	specific eddy dissipation rate ($m^2\ s^{-3}$)
S	molar entropy ($JK^{-1}mol^{-1}$)	μ	viscosity (Pa s)
T	static temperature (K)	ρ	density ($kg\ m^{-3}$)
T_0	stagnation temperature (K)	ρ_L	density of dense phase ($kg\ m^{-3}$)
T_a	ambient temperature (K)	ρ_V	density of vapour phase ($kg\ m^{-3}$)

1. Introduction

In recent years, the Carbon Capture and Storage (CCS) technique has attracted considerable attention as a method of reducing what are perceived to be excessive CO_2 concentration levels in the atmosphere. In the International Energy Agency (IEA) blue map scenario, the CCS technique is expected to contribute up to 19% reduction of CO_2 emissions by 2050 (IEA, 2010). In the CCS chain, transportation of CO_2 in high-pressure pipelines from source to storage location constitutes an important link, especially when transporting large quantities of CO_2 over long distances. It is expected that extensive networks of CO_2 pipelines would be required in the near future with the growing application of CCS (Liu et al., 2014; Mazzoldi et al., 2012).

Although pipelines are generally very safe, if an accident occurs leading to release of CO_2, the consequences may be catastrophic for human and animal populations and the environment. This is because gaseous CO_2 is

an asphyxiant that can lead to coma and even death at relatively high concentrations. Tolerable CO_2 concentration without negative environmental impact has been identified as 2,000 ppm (Mazzoldi et al., 2009). For humans, the Short Term Exposure Limit (STEL) of 15,000 ppm (1.5%) is used as a guide for maximum exposure (HSE, 2005). This is the CO_2 concentration below which no negative impact will be observed on people after a 15-minute exposure. Exposure levels above 10% will lead to rapid loss of consciousness, while further exposure at higher concentrations leads to asphyxiation or worse. In order to develop controls that may be needed to protect humans, animals and the environment from possible harmful effects of pipeline failures, it is necessary to gain a better understanding of the consequence of CO_2 released from high-pressure pipelines.

Fig. 1 shows a schematic diagram of the consequence of CO_2 released from a high-pressure pipeline. In most situations, for CO_2 transportation as either cold liquid or hot supercritical vapour, a region of two-phase flow can be initiated in the pipe by the rapid depressurisation. Following the release, the two-phase fluid expands to ambient pressure as an under-expanded jet. During the expansion the jet fluid cools down significantly due to the Joule-Thompson effect (Molag and Dam, 2011). Flashing of the liquid will occur, resulting in a two-phase jet. After flashing, the CO_2 jet will contain vapour interspersed with solid particles. For a horizontal release, some of the solid CO_2 may deposit on the ground to form a dry ice bank, while the remainder may undergo sublimation in mid-flight. The dry ice bank itself will eventually undergo sublimation due to heat transfer from the environment. This may form an additional 'source' of CO_2, affecting the downstream dispersion. As a heavier-than-air gas, CO_2 tends to slump to the ground. The near-field dispersion may be dominated by the initial momentum of the jet. After travelling for a certain distance, the cloud will lose its initial momentum and be effectively mixed with air, and disperse as a 'Gaussian' cloud. To provide sufficient separation between the CO_2 pipeline and populated areas, a quantitative analysis of the risk associated with this process is essential. This requires accurate prediction of the 'source strength' (mass flow rate) and the subsequent atmospheric dispersion using appropriate mathematical models (Koornneef et al., 2010).

In attempting to fill the knowledge gaps associated with CO_2 releases, a number of experiments were carried out in the past several years. Cosham et al. (2012a) experimentally investigated the decompression behaviour

of dense-phase pure CO_2 and various CO_2 mixtures, performed using a 144 m long, 168.3 mm internal diameter (ID) pipeline. Botros et al. (2013) tested the decompression of a CO_2-CH_4 mixture from a 38.1 mm ID, 42 m long shock tube. As the main concern in these two experiments was determination of the decompression wave speed, the pipeline pressure variation was only reported for very short time of release. Woolley et al. (2013) tested CO_2 releases using a 2 m^3 pressure vessel connected to a 9 m long discharge pipe of 50 mm ID. Apart from the variables inside the pipe and the vessel, the near-field temperature and concentration data was also measured to study the jet flow structure. Dalian University of Technology (DTU) has performed experiments on CO_2 releases from a 233 mm ID, 256 m long pipeline, using an orifice diameter of 50 mm at one end (Martynov et al., 2014). In order to provide data for the development of an outflow model, the pressure and temperature time histories were measured for much longer duration. Several CO_2 discharge and dispersion experiments have been carried out through the CO2PIPETRANS project. The first two experiments (Witlox, 2012a, b) in this project were delivered by BP and Shell respectively, featuring small-scale liquid and supercritical CO_2 releases from large storage tanks, with orifice size ranging from 1/4 inch to 1 inch. The third experiment (Witlox, 2014) was carried out by DNV GL, performed using a 50 mm ID, 200 m long pipeline containing pure CO_2 in the liquid state, released from orifices of 10 to 50 mm diameter. In these experiments, more comprehensive measurements including both discharge and dispersion data were reported. Although relatively few large-scale CO_2 releases have been investigated in the above studies, these experiments provided valuable data for model validation.

An accurate prediction of the source strength is of great importance for the modelling of the dispersion following a CO_2 release. This directly affects the risk assessment. Therefore efforts have been made to develop appropriate CO_2 pipeline discharge models. In the early stages, Bernoulli's equation and the choked flow assumption (Mazzoldi et al., 2011) have been applied to calculate the discharge velocity from high-pressure transportation facilities within CCS projects. As those equations over-simplified the physical phenomenon of the discharge process, they cannot be used to obtain a comprehensive expression of the source strength as a function of time. Picard and Bishnoi (1988) proposed a one-dimensional discharge model assuming the conservation of mass, momentum, enthalpy and energy. Using an Equation of State (EOS) for closure, the time-varying discharge of high-pressure fluid can be simulated (Mahgerefteh et al.,

2007; Mazzoldi et al., 2012). As the fluid is considered to remain at thermal and mechanical equilibrium during the decompression process, the non-equilibrium liquid/vapour transition phenomena are ignored in this model. Brown et al. (2013; 2014) proposed an improved model by introducing a 'relaxation time' to account for the non-equilibrium liquid/vapour transition. Predictions of the depressurisation of pure CO_2 showed reasonably good agreement with experimental data. However, the results were strongly dependent on the relaxation time and currently it can only be applied to the modelling of pure CO_2. For CO_2 mixtures, the two-phase region will introduce further complexities if considering the non-equilibrium phase transition. In the above studies, the Peng-Robinson (PR) EOS has been employed to model the thermodynamic properties of CO_2 as a compromise between accuracy and computational efficiency. Generally speaking, the physics involved in the high-pressure CO_2 depressurisation is still not fully understood, preventing a comprehensive estimation of the source strength for current CO_2 pipeline applications.

Interest in the heavy gas dispersion modelling has prevailed for a long time, because of the requirements for risk assessment of accidental release of hazardous gases from storage or transportation facilities. Computational Fluid Dynamics (CFD) techniques (Pontiggia et al., 2011; Scargiali et al., 2011; Sun et al., 2013; Tauseef et al., 2011) as well as analytical models (Hanna et al., 2003; Koornneef et al., 2010; Mazzoldi et al., 2011; Witlox et al., 2014) have all been widely applied. Compared to analytical models, CFD models use more detailed mathematical descriptions of the conservation principles, allowing the simulation of complex physical processes involving heat and mass transport in complicated computational domains (Scargiali et al., 2011; Sun et al., 2013). These techniques have also been used for the simulation of CO_2 dispersion in recent years, along with the increasing applications of CCS. Mazzoldi et al. (2011) simulated the dispersion of CO_2 from a 100 bar release. Results produced by two models, the heavy gas model ALOHA and the CFD model Fluidyn-PANACHE, were compared. Mazzoldi et al. (2012) investigated full-bore ruptures from various size pipelines at 10 MPa, carrying a mixture of 97% CO_2, 2% CH_4 and 1% N_2. The dispersion simulations were also carried out using Fluidyn-PANACHE. In these two studies, the authors intended to compare the models and give a general risk assessment for CO_2 transportation, rather than validating the models against measurements. Hill et al. (2011) investigated CO_2 releases from a 0.5 m diameter hole in a pipeline. Dispersion simulations were carried out using both Phast

and the CFD code ANSYS CFX. The concentrations predicted by Phast were lower than those predicted by ANSYS CFX. Solid CO_2 particles were considered in the ANSYS CFX models and their effects on the dispersion behaviour were studied using three different particle size distributions. It was found that sublimation of the solid CO_2 particles affected the dispersion behaviour, but the concentration results were not very sensitive to the particle size. Hsieh et al. (2013) studied the dispersion of CO_2 from a CCS-related infrastructure in a complex hypothetical topography. The CFD modelling approach was validated using measurements from Trials 26 and 29 of the Thorney Island experiment, two releases of a mixture of Freon-12 and N_2. In their CFD simulations of CO_2 release, they assumed a release velocity of 2.75 m s^{-1} and a small computational domain, which probably did not reflect a real release adequately. Wen et al. (2013) investigated the far-field CO_2 dispersion from a vertical vent release as well as a horizontal shock tube release. The open source CFD code OpenFOAM was employed to carry out the simulations. Results from the near-field dispersion simulations conducted by the University of Leeds were taken as the CO_2 inlet conditions. The far-field dispersion predictions of Wen et al. have shown promising agreement with the experimental data. For model validation, Witlox et al. (2014) applied Phast to simulate the CO_2 experiments carried out by BP (Witlox, 2012a) and Shell (Witlox, 2012b), which consist of a number of small-scale CO_2 releases with orifice size ranging from 1/4 inch to 1 inch. As Phast only deals with constant source strength for dispersion simulation, 20-s-averaged flow rates were applied to steady-state release trials and maximum flow rates were applied to time-varying release trials. For both experiments, Phast showed satisfactory concentration predictions. Wooley et al. (2014) simulated a hypothetical 'realistic' release from a 0.914 m diameter, 217 km long pipeline. CFD codes ANSYS CFX and FLACS were used for modelling the dispersion. They found that although significant computing resources were required, it is feasible to numerically simulate such industrially relevant flows. Overall, it seems that the current techniques are capable of modelling CO_2 dispersion for risk assessment associated with CO_2 pipelines. But comprehensive studies based on validated models on the maximum impact area due to failures of CO_2 pipelines in current CCS applications are still very limited. However, such information is likely to be very helpful for the determination of the required separation between CO_2 pipelines and residential areas.

In this paper, in order to obtain a comprehensive understanding of the consequence distance due to high-

pressure CO_2 pipeline failures, models for the predictions of source strength and atmospheric dispersion are proposed. The GERG-2008 EOS (Kunz and Wagner, 2012) was incorporated into the CFD discharge models to give precise thermodynamic property estimations. Validation of the CFD model incorporating the GERG-2008 EOS was carried out against measurements from two shock tube tests (Botros et al., 2013; Cosham et al., 2012a). The heavy gas CFD dispersion model was also validated against experimental data (Davies and Singh, 1985). Using the proposed models, release rates from full-bore ruptures of pipelines carrying typical CO_2 mixtures were predicted, and the consequence distances of CO_2 released from pipelines with various sizes and different pressures were simulated. In addition, as H_2S is a common component in the CO_2 mixture and it is harmful at very low concentration level, the impact of H_2S in a CO_2 mixture was also studied.

2. Methodology

2.1 Definition of the problem

Following the rupture of a high-pressure pipeline, a decompression wave is initiated, and propagates in the pipeline at nearly the speed of sound. Meanwhile, in the vicinity of the exit, an under-expanded jet flow exits from the orifice into the ambient with very high momentum. The prediction of highly transient high-speed flow requires a dense mesh and a very small time step (Liu et al., 2014; Novembre et al., 2006). On the other hand, dispersion modelling is space-consuming, requiring a large enough domain to allow the spread of the pollutant without the results being adversely affected by the boundary condition. For an overall CFD model including both the depressurisation and dispersion domains, the required computing time would be unacceptably long (Liu et al., 2014; Novembre et al., 2006). Therefore the problem was divided into three parts, as shown in Fig. 2.

The first part (Depressurisation) is to determine the discharge rate. This considers only the flow inside pipeline, determines features of the depressurisation procedure corresponding to the stagnation conditions (P_0 and T_0), and calculates the flow conditions at the pipe exit (P_e, T_e, and u_e). To obtain a conservative prediction of the maximum consequence distance, a full-bore rupture at one end of the pipeline was considered. For a real pipeline, the fluid will continue to flow into the pipe after the rupture has occurred until an isolation valve is closed. For simplicity, in this study the fluid was assumed to be initially at rest,

with the pipeline closed at one end and suddenly opened at the other.

Having obtained the source strength at the orifice, the jet flow conditions at ambient pressure (P_a, T_a, u_a) can be obtained using the second (Expansion) module. The values of P_a, T_a, and u_a can then be used as inlet boundary conditions for the third part, the dispersion model, in which the fluid can be treated as incompressible.

In this study, simulations of the discharge and dispersion (the first and third parts) were carried out using the commercial CFD code ANSYS Fluent. The under-expanded flow within the atmospheric expansion region (the second part) was modelled using simplified conservation equations to avoid resolving the high pressure gradients as well as the possible dry ice formation.

2.2 Real gas model for source strength prediction

A realistic simulation of the depressurisation inside the pipeline is important to correctly reflect the source strength of CO_2 released from high-pressure pipelines. This requires precise modelling of the thermodynamic properties of CO_2 using a 'real gas' EOS (Liu et al., 2014). The first real gas EOS was developed by van der Waals in 1873 (van der Waals, 1873). Subsequently, a number of EOSs have been developed in order to accurately predict the thermodynamic properties of fluids. These EOSs can be divided into two categories (Li et al., 2011): (1) 'cubic' equations with simple form, such as those due to Redlich and Kwong (RK) (Redlich and Kwong, 1949), Soave, Redlich and Kwong (SRK) (Soave, 1972), Patel and Teja (PT) (Patel and Teja, 1982), Peng and Robinson (PR) (Peng and Robinson, 1976) and many others; and (2) equations with more complex structures, such as those due to Benedict, Webb and Rubin (BWR) (Benedict et al., 1940), Lee and Kesler (LK) (Lee and Kesler, 1975), the GERG EOS (Kunz and Wagner, 2012; Wagner, 2009), etc. EOSs with more complex structure may give better estimations of some specific properties, but they are usually more difficult to implement due to their complicated calculation procedure, particularly if they are not already included in the original simulation code.

In this study, the GERG-2008 EOS (Kunz and Wagner, 2012) was employed. GERG-2008 EOS is an extended version of GERG-2004 developed by the Groupe Européen de Recherches Gazières (GERG). The GERG-2008 EOS is valid for wide ranges of temperature (from 90 K to 450 K) and pressure (up to 35 MPa),

and covers the gas phase, the liquid phase, the supercritical region, and vapour-liquid equilibrium states for natural gases and other mixtures consisting of up to 21 components: methane, nitrogen, carbon dioxide, ethane, propane, n-butane, isobutane, n-pentane, isopentane, n-hexane, n-heptane, n-octane, hydrogen, oxygen, carbon monoxide, water, helium, argon, n-nonane, n-decane, and hydrogen sulphide. Currently, the GERG-2008 EOS is considered to be a reference EOS for gas pipelines (Cosham et al., 2010).

ANSYS Fluent supports User-Defined Real Gas Model (UDRGM) implemented through User-Defined Functions (UDFs) (ANSYS, 2011b). In the UDRGM, physical properties of the fluid can be estimated at runtime using a real gas EOS. For given pressure and temperature (P-T), the thermodynamic properties required for a real gas model in Fluent include density, enthalpy, entropy, speed of sound, specific heat, molecular weight, partial derivative of density with respect to temperature and pressure, and partial derivative of enthalpy with respect to pressure.

The GERG-2008 package provides a dynamic link library, including a set of subroutines for the calculation of properties at given P-T values for any CO_2 mixture (Wagner, 2009). In the pipeline, a homogenous equilibrium fluid was assumed. Thus in the UDRGM the library could be called to calculate the properties at each node in a flow domain. In this work, instead of a direct call to the library at runtime, pre-compiled property tables for all the required thermodynamic properties generated by the GERG-2008 EOS were used and a linear interpolation scheme was implemented to obtain properties at any P-T point. Compared to direct calls to the library, locating the P-T point within the preloaded property tables and using linear interpolation are much more time-efficient. A performance test of UDFs for obtaining thermodynamic properties at any P-T point during the simulation showed that the proposed method is about 20 times faster than a direct call to the library. Furthermore, the problems of the GERG-2008 library which occasionally fails to produce some properties at certain P-T values and enters an infinite optimisation loop that causes the library to crash can be avoided. The speed of sound in the two-phase region has not been defined in the GERG-2008 library. However, as a homogenous equilibrium fluid was assumed, the definition of speed of sound for a single phase fluid could be used. The speed of sound in the two-phase region was defined as:

$$w = \sqrt{\left.\frac{\mathrm{d}P}{\mathrm{d}\rho}\right|_S} \tag{1}$$

where ρ is the density and S the entropy.

Using the above method, for any CO_2 mixture, according to the stagnation conditions, structured two-dimensional arrays for the required properties for chosen ranges of pressure and temperature could be established. To ensure precision and a smooth variation of the property value, the tables can be made dense enough, especially for the region near the phase boundary.

The performance of the GERG-2008 EOS coupled CFD model was validated through simulations of two shock tube tests. The first test ('case A') was conducted at the TransCanada pipeline Gas Dynamics Test Facility in Didsbury, Alberta, Canada (Botros et al., 2013). The shock tube used in case A was 42 m long, with an internal diameter (ID) of 38.1 mm. The working fluid was a binary mixture: CO_2 72.6% and CH_4 27.4%. The stagnation conditions are: P_0 = 28.568 MPa, and T_0 = 313.65 K. The second test ('case B') was carried out by the National Grid at GL Noble Denton's Spadeadam Test Site in Cumbria, UK (Cosham et al., 2012a). The pipe used in case B was 144 m long, with an ID of 146.36 mm. The working fluid was a 5-component mixture: CO_2 91.03%, H_2 1.15%, N_2 4%, O_2 1.87% and CH_4 1.95%. The stagnation conditions of case B are: P_0 = 15.05 MPa, and T_0 = 283.15 K.

Fig. 3 shows the predicted decompression wave speed against the measurements. The results indicate that CFD model using GERG-2008 EOS performs very well. In case A (see Fig. 3a), the predicted wave speed is consistent with the measurements nearly in the entire pressure range. The abrupt drop in the measured decompression wave speed curve which created a pressure plateau was predicted successfully. In case B (see Fig. 3b), the pressure plateau was also predicted and the length of the plateau is consistent with the measured data. But there is a larger discrepancy between the predicted and measured decompression wave speed. This discrepancy may result from the homogenous equilibrium assumption applied to the model (Brown et al., 2013; Cosham et al., 2012b). Consequently, the non-equilibrium liquid/vapour transition phenomena which can influence the results to various degrees could not be accounted for in the simulations. In both shock tube tests, the CO_2 inside the pipe experienced phase change. But as the mixture used in case B was much richer in CO_2, the results may be affected to a larger extent. However, the predicted flow variables close to the exit

(the left end of the decompression wave speed curve) in both cases are very close to the experimental data, which is more important for source strength prediction, and therefore relevant to the dispersion problem.

2.3 Atmospheric expansion model

After exiting from the orifice, the flow presents as an under-expanded jet with very high momentum and reaches ambient pressure very soon (Liu et al., 2014). An atmospheric expansion model is required to bring the flow conditions at the pipe exit to the plane where the jet pressure reaches ambient value to provide a 'pseudo source' for the dispersion model (refer to Fig 2). To avoid resolving the high pressure gradient as well as the possible dry ice formation within the expansion region, the under-expanded flow was modelled using simplified conservation equations to compute approximately the equivalent area of the pseudo source corresponding to the area of the pipe exit.

In the expansion region, the air entrainment, viscous force, and heat transfer between the jet and atmosphere are assumed negligible. Birch et al. (1987) have applied the conservation of mass and momentum to obtain the flow conditions after expansion. They also assumed that the fluid will regain its original stagnation temperature rapidly, so that $T_a \approx T_0$ (refer to Fig. 2). Thus the density of the fluid at the atmospheric pressure plane can be pre-determined using an appropriate EOS. However, this assumption contradicts experience. Experimental measurements (Wareing et al., 2014) indicated that for a dense-phase CO_2 release, the jet temperature will reach the freezing point and maintained a certain distance downstream from the jet exit. Sand et al. (Sand et al., 1996) extended the model by Birch et al. by including an enthalpy equation and thereby making the unrealistic assumption of recovered temperature at the pseudo source plane unnecessary.

In this study, the model used by DNV Phast was employed. Phast is a hazard analysis software tool, which can examine the progress of a potential incident from the initial release to far field dispersion (Witlox et al., 2009). Phast provides an ATmospheric EXpansion module (ATEX) to model the expansion of a continuous release from the conditions in the leak orifice down to atmospheric pressure. Along the expansion zone one-dimensional homogeneous flow is assumed in thermal equilibrium and with zero air entrainment. The unknown post-expansion data are then set from the pre-expansion data by imposing three conservation equations (conservation of mass, momentum, and energy) and two equations of properties (equations for

density and enthalpy) (DNV, 2011):

$$\rho_a A_a u_a = \rho_e A_e u_e \tag{2}$$

$$\rho_a A_a u_a^2 = \rho_e A_e u_e^2 + (P_e - P_a) A_e \tag{3}$$

$$\rho_a A_a u_a \left(h_a + \frac{1}{2} u_a^2 \right) = \rho_e A_e u_e \left(h_e + \frac{1}{2} u_e^2 \right) \tag{4}$$

$$\rho = \rho(P, T; f_L) = f_L \rho_L(P, T) + (1 - f_L) \rho_V(P, T) \tag{5}$$

$$h = h(P, T; f_L) = f_L h_L(P, T) + (1 - f_L) h_V(P, T) \tag{6}$$

where A is the area, h the specific enthalpy, and f the phase fraction; subscripts L and V denote dense phase and vapour phase respectively.

In the above equations, the density and enthalpy are estimated using GERG-2008 EOS. Clearly, this model has the advantage of calculating phase fractions. If the pressure and temperature at the orifice can be predicted, applying the homogeneous equilibrium assumption, phase fractions at the orifice and the ambient pressure plane can all be predicted.

2.4 Numerical methods for dispersion simulation

The dispersion simulations were carried out using ANSYS Fluent, which solves the Reynolds-Averaged mass, momentum, energy and scalar transport equations. The extensively validated k-ε model was used for representing the effects of turbulence. This model introduces two transport equations for Turbulent Kinetic Energy (TKE, k) and Eddy Dissipation Rate (EDR, ε) respectively:

$$\frac{\partial}{\partial t}(\rho k) + \frac{\partial}{\partial x_i}(\rho k u_i) = \frac{\partial}{\partial x_j}\left[\left(\mu + \frac{\mu_t}{\sigma_k} \right) \frac{\partial k}{\partial x_j} \right] + G_k + G_b - \rho\varepsilon \tag{7}$$

$$\frac{\partial}{\partial t}(\rho \varepsilon) + \frac{\partial}{\partial x_i}(\rho \varepsilon u_i) = \frac{\partial}{\partial x_j}\left[\left(\mu + \frac{\mu_t}{\sigma_\varepsilon} \right) \frac{\partial \varepsilon}{\partial x_j} \right] + C_{1\varepsilon} \frac{\varepsilon}{k} G_k - C_{2\varepsilon} \rho \frac{\varepsilon^2}{k} \tag{8}$$

where u_i is the velocity component along x_i direction, t the time, μ the viscosity, μ_t the turbulent viscosity ($\mu_t = c_\mu k^2/\varepsilon$), and G_k the generation of turbulence kinetic energy due to the mean velocity gradients. The constants in Eqs. (7) and (8) are: $c_\mu = 0.09$, $C_{1\varepsilon} = 1.44$, $C_{2\varepsilon} = 1.92$, $\sigma_\varepsilon = 1.3$, and $\sigma_k = 1.0$.

Wind velocity is one of the most significant parameters in dispersion modelling, as it determines how

quickly the pollutant will be diluted by the flowing air. In order to account for the variation in wind velocity with elevation near the ground level due to frictional effects, a power law is used to describe the vertical wind profile (Peterson and Hennessey, 1978):

$$u = u_r \left(\frac{z}{z_r} \right)^{\alpha} \tag{9}$$

where u is the wind velocity at height z, u_r a reference wind velocity measured at the reference height z_r, and α the 'wind shear exponent', which depends upon the atmospheric stability class and the ground surface roughness.

In order to achieve and maintain appropriate levels of TKE and EDR throughout the domain, it is necessary to specify these parameters at the inlet. In the present study, the TKE and EDR profiles suggested by Han et al. (2000), which are based on a similarity theory and has reasonable agreement with measured data, were used. The k and ε are specified by:

$$k = 6u_*^2 \tag{10}$$

$$\varepsilon = \frac{u_*^3}{Kz}\left(1.24 + 4.3\frac{z}{L} \right) \tag{11}$$

where u_* is the friction velocity, L the 'Monin-Obukhov' length, and K the von Karman constant (≈0.4).

As the ground texture may affect the turbulence level, the roughness of the corresponding boundary should be specified in the CFD code. In ANSYS Fluent, the wall roughness is defined in terms of an equivalent sand-grain roughness height K_S and a roughness constant C_S, which are related by (ANSYS, 2011a; Blocken et al., 2007):

$$K_S = \frac{9.793 z_0}{C_S} \tag{12}$$

where z_0 is the surface roughness length.

The numerical methods adopted here were validated through a simulation of Trial 26 of the Thorney Island field experiment. The Thorney Island tests (Davies and Singh, 1985) were designed to study the dispersion of dense gas clouds which might result from catastrophic releases. In Trial 26, the gas source was a

cylindrical tent of 14 m diameter, 13 m height and total volume of about 2000 m^3, made from flexible material, which was left to collapse to the ground at the beginning of the trial. An obstacle measuring 9 m × 9 m × 9 m was situated 50 m downwind from the cylindrical gas tent. The composition of the released gas was 68.4% N_2 and 31.6% Freon 12, with a relative density of 2.0. Although the tracer gas was not CO_2, these experiments can still be used to validate the CO_2 dispersion model because the dispersion behaviour of heavy gases should be similar. Furthermore, the gas cylinder contained nearly 5000 kg pollutant, making it appropriate for the validation of the CFD model simulating a large release. Fig. 4 shows the schematic of Trial 26 and part of the surface mesh, including the ground, gas cylinder, and building (obstacle), and the mesh refinement (in Fig. 4b, a part of the mesh has been cut off because of long distance to the outlet).

In the experiment, there were two concentration sensors mounted on the obstacle: on the windward face at a height of 6.4 m, and on the leeward face at a height of 0.4 m from the ground. Fig. 5 plots the measured and predicted gas concentration time histories. For comparison, the results predicted by Hsieh et al. (2013) are also shown. It is found that the predicted maximum concentrations are close to the measurements with reasonable deviations at both monitor locations. The time variations in the concentrations at both monitor locations are also well reflected by the simulation in this work. On the contrary, the peak concentration on the windward face was not predicted by Hsieh et al., as the initially sharp rise and fall of the concentration was not reflected in their predictions. The concentration on the leeward face predicted in this study also has better agreement with the measurements. The larger discrepancies between measurements and the results predicted by Hsieh et al. may be mainly due to the mesh quality. In their model, the mesh was not refined near the windward face of the obstacle, leading to poor prediction of gas concentration on the windward face. The concentration on the leeward face was predicted much better by Hsieh et al, owing to the mesh refinement near the leeward face. In addition, for a large release, it is also important to ensure a large enough computational domain to minimise the impact of the boundary conditions. In the simulation presented in this paper, the computational domain measures 300 m (length) × 260 m (breadth) × 80 m (height), which is much larger than 147 m × 126 m × 40 m used by Hsieh et al. Overall, the good agreement between the CFD results and experimental data proved the capability of the methods adopted here for the prediction of dispersion following release of a large amount of heavy gas.

3. CFD models

3.1 Discharge model

As mentioned above, a full-bore rupture at one end of the pipeline was considered in the present work to obtain a conservative prediction. A one-dimensional mesh was employed to minimise the computing time. GERG-2008 EOS was incorporated into the CFD model to calculate the thermodynamic properties.

Fig. 6 shows schematically the one-dimensional mesh of a 5 km long pipeline. Close to the exit, within 100 m, the width of the element is 0.01 m, gradually increasing to a maximum 0.1 m at the closed far end. The 'symmetry' condition was applied to the two lateral sides. An ambient pressure (zero gauge pressure) boundary condition was applied at the pipe exit. The pipe closed end was defined as a no-slip wall.

The density-based solver was selected for the solution, as it was originally designed for high-speed compressible flows. Although in the CFD code used in this study, the pressure-based solver is applicable to a broad range of flows, the origins of the density-based formulation may give it an accuracy advantage over the pressure-based solver for high-speed compressible flows (ANSYS, 2011a). Another advantage of the density-based solver is that it can correctly predict the choke conditions at the pipe exit during the depressurisation, disregarding the initial boundary settings at the pipe exit which are ambient pressure and temperature. The Advection Upstream Splitting Method (AUSM) was chosen for flux type and a second order upwind method was specified for spatial discretisation. The convergence criterion was defined as the residuals becoming equal or less than 10^{-4}.

It should be noted that the one-dimensional model cannot account for friction. Also the outflow velocity is considered to be uniformly over the exit plane. These simplifications will result in over-prediction of the source strength. However for risk assessment, a conservative prediction is usually acceptable.

3.2 Dispersion model

In the dispersion model, the computational domain shown in Fig. 7a was used. The dimensions of the computational domain are 1500 m (length) × 600 m (breadth) × 200 m (height). A horizontal release parallel to the wind direction was assumed to account for the worst case. The diameter of the CO_2 source plane depends on the release rate, velocity and density. The computational domain was discretised in the form of

hexahedral cells (see Fig. 7b), with refinement around the CO_2 source and also near the ground (in Fig. 7b, a part of the mesh has been cut off because of long distance to the outlet), which makes a grid with nearly 2 million cells to enable accurate prediction of flow parameters.

In the dispersion model, seven boundary conditions were required to be defined: (1) wind inlet, (2) CO_2 inlet, (3) ground, (4) left side, (5) right side, (6) top, and (7) outlet of the computational domain. The CO_2 inlet was specified by a mass flow rate. The 'top' and two 'side' boundaries were defined as impermeable 'symmetry' boundaries with zero normal velocity and zero gradients of all variables, and zero fluxes of all quantities across it. The outlet was set as a pressure boundary with ambient pressure and temperature. The ground boundary was defined as a no-slip, isothermal wall with temperature equal to the ambient temperature.

4. Results and discussion

4.1 Source strength from full-bore rupture

To understand the variations of the flow variables inside the pipeline after an accidental release, a 5 km long pipeline subjected to a full-bore rupture at one end was simulated at first using the one-dimensional CFD model. The fluid inside the pipeline was the CO_2 mixture used in the shock tube test Case B (Section 2.2). The stagnation conditions were also considered the same as in the shock tube test Case B, with P_0 = 15.05 MPa and T_0 = 283.15 K.

Fig. 8 shows the predicted pressure and flow velocity along the 5 km pipeline at different times. At the moment of a rupture, the pipe starts to depressurise. The decompression wave moves away from the pipe exit at the sonic speed of the fluid at stagnation conditions (w_0: 523.6 m s^{-1}). Following its decompression path (refer to Fig. 9), the fluid depressurises to the saturation state at first, resulting in a plateau with the conditions at the phase boundary (P = 8.1 MPa, T = 275.8 K) extending along the pipe (see Figs. 8a and 8b). Over the width of the plateau, the fluid is still in 'liquid' state, maintaining a stable thermodynamic state and a constant flow velocity (u_o: 17.2 m s^{-1}). At the rupture end, the fluid depressurises from the saturation state, leading to a two-phase flow in the pipe. As the sonic speed of the gas-liquid mixture (w_m: around 92 m s^{-1}) is relatively low, the propagation of the two-phase flow from the rupture end is relatively slow at the sonic speed relative to the fluid flow velocity (w_m - u_o, see Figs. 8a to 8c).

The decompression wave will eventually reach the end of the pipe (at 9.5 s) and will be reflected back. Soon after the arrival of the decompression wave at the closed pipe end, the plateau with saturation conditions will also reach the closed end of the pipe. After this moment, a two-phase flow is also initiated from the close end of the pipe, propagating to the open end at the sonic speed relative to the flow velocity ($w_m + u_o$). At about 38 s, it will meet the two-phase flow initiated from the rupture end (Fig. 8d). After that, the reflected decompression wave keeps travelling towards the open end, but with a higher velocity as the subsequent flow velocity, u_o, is much higher than the constant flow velocity in the range of the plateau.

During the above process, the flow is 'choked' at the exit until the reflected decompression wave reaches the exit at about 45 s. For this condition, the choke pressure and temperature are 4.18 MPa (Figs. 8a to 8e) and 261.1 K respectively. The flow velocity at the exit is also maintained at Mach 1. After the decompression wave has been reflected back from the closed end and reaches the exit, the choke state ceases to exist and the choke pressure at the exit can no longer be maintained (Fig. 8f). Clearly, before the reflected decompression wave reaches the exit, a constant mass flow rate will be obtained at the pipe exit, as the flow variables at the exit are constant. This is reflected in Fig. 10 showing the predicted discharge mass flux at the rupture.

The above analysis is based on the one-dimensional CFD simulation, without the considerations of friction of the pipe wall and heat transfer between the fluid and the environment. These factors will cause the heating up of the fluid near the wall, especially for the region close to the exit where there exists the highest flow velocity and lowest fluid temperature. The depressurisation of the fluid will then deviate from its original path and the pressure at the exit will gradually decrease. In reality, the discharge rate will reach the release rate predicted by the one-dimensional CFD model immediately after rupture, but subsequently, because of the mentioned effects, it will gradually decrease. A simulation with two-dimensional grid has been carried out for a release of 5 seconds. It was found that, at 5 s, compared with the results of the two-dimensional simulation, the one-dimensional simulation overestimated the cumulative released mass by 15%. Although the mass flow rate is over-predicted by the one-dimensional CFD model, assuming this value as a 'nominal' discharge rate for the dispersion modelling is appropriate, as for risk assessment, a conservative prediction of the consequence distance is usually acceptable. Moreover, the one-dimensional CFD model is much more time-efficient than a two-dimensional model considering friction and heat transfer. In engineering

applications, usually a pipeline measuring tens of kilometres in length is required to evaluate the risk. For example, in the Australian Standard, a 50 km long pipeline is used (Standards Australia, 2012). However, in view of the depressurisation of the CO_2 pipeline as revealed by the CFD simulation shown in Fig. 8 and Fig. 10, a much shorter pipe can be used for the source strength prediction and a quick estimation of the nominal discharge rate for dispersion modelling is possible.

The composition of the CO_2 stream transported in the pipeline for CCS will depend on its source. There are three main process routes for capturing CO_2 from a power plant: post-combustion, pre-combustion and oxyfuel. Table 1 lists three typical compositions of CO_2 mixtures captured from the three process routes (Seevam et al., 2010), representing typical CO_2 mixture compositions for Australian conditions.

From Table 1, we note that for Australian conditions, the streams from all three capture processes are CO_2-rich mixtures and the major impurities include N_2, O_2, CH_4, H_2 and Ar. Binary CO_2 mixtures with various fractions of these five impurities were investigated and the predicted source strength from full-bore rupture of pipelines carrying these binary mixtures was estimated for three values of the stagnation pressure (10 MPa, 15 MPa and 20 MPa). The results are shown in Fig. 11. The stagnation temperature was assumed to be 20 ºC for all cases.

The general trend is that a higher fraction of impurity yields higher discharge rate. This is mainly because of the higher speed of sound with higher fraction of impurity in the mixture. Although a higher fraction of impurity will result in a lower density for the binary mixture (the densities of the impurities are lower than the density of CO_2 in both liquid and gas states), the decrease in mixture density is outweighed by the increase in the sonic speed. At a higher stagnation pressure, the fluid will choke at a correspondingly higher pressure at the exit, resulting in higher density. This results in the increase of the discharge rate as shown in Fig. 11. However the increase is not so significant because the speed of sound is lower at higher pressure due to higher liquid fraction.

It is also found that the sensitivity of the discharge rate to the fraction of different impurities is different. The fraction of H_2 has the most influence on the discharge rate while the fraction of CH_4 has the least influence. This is because that the magnitude of the shift of the ‘bubble curve’ corresponding to the various impurities

to pure CO_2 is different. As shown in Fig. 12, the CO_2-H_2 mixture (pink dotted line) has the widest two phase region while the CO_2-CH_4 mixture has the narrowest phase envelope (blue dotted line). Clearly, the shift of the bubble curve will change the decompression path (refer to Fig. 9) and affect the choke conditions. Furthermore, when the fluid is choked in the two phase region, a narrower phase envelope implies that the choke pressure cannot be changed significantly when the fraction of the impurity is changed, as the change in the choke temperature is also limited. If the depressurisation is initiated from P = 15 MPa and T = 30 ºC, for a CO_2-H_2 mixture, the choke pressure and temperature for 1% and 5% H_2 are (3.4 MPa, 268.9 K) and (4.3 MPa, 269.4 K) respectively, while for a CO_2-CH_4 mixture, they are (3.2 MPa, 268 K) and (3.6 MPa, 266.5 K) respectively.

To evaluate the risk associated with CO_2 pipelines transporting the typical CO_2 mixtures for Australian conditions shown in Table 1, the discharge flow parameters corresponding to these mixtures were estimated, as shown in Table 2. The stagnation temperature was set as 20 ºC. Three stagnation pressures from 10 to 20 MPa were evaluated. As the values for discharge variables of Pre-combustion and Oxyfuel are very similar, we only considered the Pre-combustion and Post-combustion mixtures in the subsequent analysis.

In order to take the discharge variables to the inlet surface of the dispersion model, the methodology introduced in Section 2.3 was applied to solve the flow variables at the atmospheric pressure plane. The phase fraction at the exit was estimated by flash calculation of GERG-2008 library, assuming a vapour-liquid equilibrium state. Table 3 shows the phase fractions at the exit, as well as the phase fractions, density and velocity at the inlet boundary of the computational domain used for the dispersion model, for full-bore rupture of pipelines carrying typical CO_2 mixtures initiated from different stagnation pressures.

4.2 Dispersion simulation

Following the estimation of the discharge flow parameters, dispersion simulations using the predicted source strength for both pre-combustion and post-combustion CO_2 mixtures were carried out, for stagnation pressures of 10 MPa, 15 MPa and 20 MPa. Table 4 shows the health impact of CO_2, in which two CO_2 concentration levels (50,000 ppmv and 80,000 ppmv) are considered relevant for determining the hazard posed by the dispersion. The downstream consequence distance was determined as the maximum distance

from the pipe rupture bounded by two concentration envelopes corresponding to these two concentration levels.

Simulations showed that for a given concentration level, the consequence distance will reach a stable value after a short period of time. Fig. 13 shows the consequence distance time histories of the 50,000 ppm and 80,000 ppm envelopes (400 mm ID pipeline, 15 MPa, post-combustion, solid particles considered). The 50,000 ppm envelope reached the stable distance within 30 s, while the 80,000 ppm reached the stable distance much faster. This phenomenon would be very helpful because it makes a quantitative risk assessment possible.

In the CFD code, a two-phase inflow of CO_2 can be simulated using a 'Discrete Phase Model' (DPM) (ANSYS, 2011a). This is a Langrangian particle tracking method and the CO_2 solid particles can be modelled as 'droplets'. If the DPM is used, the sublimation of solid CO_2 will depend on the heat transferred from the environment, which can be handled by the CFD code with appropriate settings. It should be noted that the consequence distance vs time histories shown in Fig. 13 were obtained with the application of DPM. Alternatively, we can also consider an 'all-gas' dispersion model, assuming that all the fluid at the CO_2 source plane is in the vapour state.

Fig. 14 compares the consequence distances obtained by these two methods (400 mm ID pipeline, 15 MPa, post-combustion). Notably, in the DPM simulations, the effects of particle size on the dispersion have been investigated using four droplet diameters: 10, 50, 100 and 150 μm. It was found the particle size has negligible influence on the dispersion, which is consistent with the results obtained by Hill et al. (2011). Clearly, the consequence distance obtained by the 'all-gas' model is much longer than that obtained by DPM. This is because the sublimation of the solid particles relies on the heat transfer, resulting in a slow phase change rate (Mazzoldi et al., 2008). In order to remove the uncertainties of considering dry ice sublimation and to obtain conservative predictions, in the subsequent simulations for risk assessment, 'all-gas' models were used.

Fig. 15 shows the predicted consequence distances following full-bore rupture of a CO_2 pipeline with ID varying from 400 mm to 800 mm. For a certain stagnation pressure, it is seen that the consequence distance

varies almost linearly with pipe size (ID). Also, a higher stagnation pressure results in a larger impact area due to the higher discharge rate. In comparison with the increase in the stagnation pressure, the increase in the consequence distance is not so significant, especially when raising the stagnation pressure from 10 MPa to 15 MPa. For a pipeline with 600 mm ID carrying pre-combustion CO_2 mixture (Fig. 15a), when the pressure is increased from 10 MPa to 15 MPa, the pressure is raised by 50%, but the increase in the consequence distance corresponding to 50,000 ppm concentration is only 2%. Although the increase in the consequence distance for 50,000 ppm concentration is 10% when increase the pressure from 15 MPa to 20 MPa, it is still much lower than the 33% increase in the stagnation pressure. The fact that more increase in the consequence distance was observed when raising the stagnation pressure from 15 MPa to 20 MPa, compared to the increase of stagnation pressure from 10 MPa to 15 MPa, may be due to the greater increase in the discharge rate and also less reduction in the discharge velocity for stagnation pressure from 15 MPa to 20 MPa (refer to Tables 2 and 3).

Fig. 16 compares the consequence distances between pre-combustion and post-combustion CO_2 mixtures for stagnation pressure of 15 MPa. The release of pre-combustion CO_2 mixture has larger consequence distances because of the higher discharge velocity and net CO_2 release rate.

For small releases with low momentum, high wind speed helps the dispersion, because increasing the wind speed enhances mixing and transport. But for these large horizontal releases with high momentum, the CO_2 initially accumulates on the ground and the dispersion may be dominated by the source momentum. Under these conditions, the wind may drive the CO_2 cloud further downstream. Higher wind velocity may result in longer consequence distances. But the effect of wind velocity is limited as the amount of CO_2 released is very large and the wind velocity is usually much lower than the discharge velocity. In the aforementioned case for 400 mm ID pipeline with 10 MPa stagnation pressure, the wind velocity at 10 m height was specified as 2 m s^{-1}, but the jet velocity 324 m downstream from the rupture (the consequence distance corresponding to 50,000 ppm concentration) at 10 m height is 12 m s^{-1}, which is still much higher than the inflow wind velocity. In Fig. 17, the consequence distances predicted using wind velocities of 2 m s^{-1} and 5 m s^{-1} are compared (post-combustion mixture; wind velocities were applied at 10 m height). When the wind velocity is increased from 2 m s^{-1} to 5 m s^{-1}, the CO_2 concentration envelope can be enlarged by 2% to 7%.

4.3 Effect of Hydrogen Sulphide (H_2S)

The fluid transported in the pipeline may contain H_2S at concentrations that are hazardous if dispersed in the atmosphere, to the extent that the toxicity of H_2S may pose a greater hazard than the asphyxiating effect of the CO_2 itself. This is because H_2S is harmful even at very low concentration levels (see Table 5).

The concentration of H_2S in a typical pre-combustion CO_2 mixture shown in Table 1 appears too low to be a hazard comparable to CO_2. However, it is still possible that CO_2 mixtures from different sources contain higher H_2S fractions. For example, the 300 km, 305-356 mm ID Weyburn Pipeline (Metz et al., 2005) carries more than 5,000 tonnes day^{-1} of CO_2 from the Great Plains Synfuel Plant near Beulah, North Dakota to the Weyburn Enhanced Oil Recovery (EOR) project in Saskatchewan. The composition of the gas carried by the Weyburn pipeline is typically CO_2 96%, H_2S 0.9%, CH_4 0.7%, C2+ hydrocarbons 2.3% and CO 0.1%.

As the initial fraction of H_2S in the Weyburn pipeline is 9,000 ppm, it may present a great hazard if allowed to disperse in the atmosphere. The dispersion of this mixture was therefore investigated using the proposed models. For comparison, the risk of H_2S at 200 ppm is assumed to be equivalent to that of CO_2 at 50,000 ppm, while 500 ppm H_2S corresponds to 80,000 ppm CO_2.

For a 400 mm ID pipeline, if the stagnation pressure and temperature are 15 MPa and 20°C respectively, the predicted release rate for full-bore rupture at one end is 3350 kg s^{-1}. Using this release rate, a dispersion simulation was carried out and Fig. 18 shows the obtained impact distances for both H_2S and CO_2. Clearly, for the CO_2 mixture carried by the Weyburn pipeline, if a rupture occurs, the H_2S may cause much greater hazard than the CO_2 itself.

In order to estimate the fraction level for which the consequence distance of H_2S will be greater than that of CO_2, dispersion simulations with various fraction levels of H_2S, from 0.3% to 0.9%, were carried out for a full-bore rupture at one end of a 400 mm ID pipeline.

Fig. 19 shows the consequence distances for different H_2S levels. For a 500 ppm H_2S envelope, the threshold source fraction of H_2S is 0.6%, below which the 500 ppm H_2S envelope will be enclosed by the 80,000 ppm CO_2 envelope. For 200 ppm H_2S envelope, the threshold source fraction of H_2S is 0.4%.

5. Conclusions

In this study, a method for estimating the consequence distance following CO_2 releases from high-pressure pipelines is proposed. The method uses both analytical and CFD techniques. The GERG-2008 EOS was incorporated into the CFD code to predict the discharge rate. Two shock tube tests were simulated to validate the CFD models using the GERG-2008 EOS. An analytical model was applied to estimate the atmospheric expansion, which provides the necessary input (flow parameters at the inlet boundary) for the dispersion simulation. One of the Thorney Island experiments was simulated for the validation of the heavy gas dispersion model. Using the proposed models, full-bore releases from CO_2 pipelines of various sizes at different stagnation pressures were simulated. It can be concluded that:

(1) In conjunction with the GERG-2008 EOS, the CFD model is able to simulate the depressurisation of high-pressure pipelines carrying CO_2 mixtures. For simplicity, non-equilibrium liquid/vapour transition phenomena were not considered during the depressurisation, and may cause discrepancy in the estimation of the decompression wave speed. A higher CO_2 fraction in the mixture will result in relatively higher discrepancy. However, the overall performance is satisfactory and the model can be used to predict the discharge rate due to accidental release.

(2) During the depressurisation following a full-bore rupture, the decompression wave propagates at sonic speed in the pipeline. If the effects of friction and heat transfer from the environment are ignored, a choked flow with constant flow variables will be maintained at the pipe exit until the decompression wave is reflected back to the exit.

(3) For impurities typical in current CCS applications, a higher fraction of impurity in CO_2 mixtures usually results in higher discharge rate, owing an increased speed of sound. Different impurities will affect the discharge rate to different extent, mainly depending on the magnitude of the shift of the bubble curve. Compared to N_2, O_2, CH_4 and Ar, the existence of H_2 in CO_2 mixtures has a maximum impact on the discharge rate.

(4) Consequence distances for CO_2 pipelines carrying typical CO_2 mixtures of various sizes and different stagnation pressures were obtained, considering full-bore rupture. These distance estimates can be used to determine the ‘measurement length’ before the deployment of CO_2 pipelines.

(5) If the CO_2 stream contains H_2S, the H_2S may present a greater hazard than the CO_2 itself. The threshold value of the fraction of H_2S is 0.4%. If the fraction of H_2S is less than 0.4% at the source, after rupture the 200 ppm H_2S envelope will be contained within the 50,000 ppm CO_2 envelope.

6. Acknowledgements

This work is being carried out under the aegis of the Energy Pipelines Cooperative Research Centre (EPCRC), supported through the Australian Government's Cooperative Research Centre Program, and funded by the Department of Resources, Energy and Tourism (DRET). Cash and in-kind support from the Australian Pipelines Industries Association Research and Standards Committee (APIA RSC) is gratefully acknowledged.

References

ANSYS, 2011a. ANSYS FLUENT theory guide. ANSYS Inc., USA.

ANSYS, 2011b. ANSYS FLUENT UDF Manual. ANSYS Inc., USA.

Benedict, M., Webb, G.B., Rubin, L.C., 1940. An empirical equation for thermodynamic properties of light hydrocarbons and their mixtures. J Chem Phys 8, 334-345.

Birch, A.D., Hughes, D.J., Swaffield, F., 1987. Velocity decay of high pressure jets. Combustion Science and Technology 52, 161-171.

Blocken, B., Stathopoulos, T., Carmeliet, J., 2007. CFD simulation of the atmospheric boundary layer: wall function problems. Atmos Environ 41, 238-252.

Botros, K.K., Jr, E.H., Craidy, P., de Janeiro, R., 2013. Measuring decompression wave speed in CO2 mixtures by a shock tube, Pipelines International, pp. 22-26.

Brown, S., Martynov, S., Mahgerefteh, H., Chen, S., Zhang, Y., 2014. Modelling the non-equilibrium two-phase flow during depressurisation of CO2 pipelines. International Journal of Greenhouse Gas Control 30, 9-18.

Brown, S., Martynov, S., Mahgerefteh, H., Proust, C., 2013. A homogeneous relaxation flow model for the full bore rupture of dense phase CO2 pipelines. International Journal of Greenhouse Gas Control 17, 349-356.

Cosham, A., Boreas, A., Eiber, R.J., Clark, E.B., 2010. GASDECOM: Carbon dioxide and other components, The 8th International Pipeline Conference (IPC2010). ASME, Calgary, Canada, pp. 777-794.

Cosham, A., Jones, D.G., Armstrong, K., Allason, D., Barnett, J., 2012a. The decompression behaviour of Carbon Dioxide in the dense phase, The 9th International Pipeline Conference (IPC2012). ASME, Calgary, Canada, pp. 447-464.

Cosham, A., Jones, D.G., Armstrong, K., Allason, D., Barnett, J., 2012b. Ruptures in gas pipelines, liquid pipelines and dense phase carbon dioxide pipelines, The 9th International Pipeline Conference (IPC2012). ASME, Calgary, Canada, pp. 465-482.

Davies, M.E., Singh, S., 1985. The phase II trials: a data set on the effect of obstructions. J Hazard Mater 11, 301-323.

DNV, 2011. ATEX Theory Document. DNV Software, London.

Han, J.A., Pal, S., Shen, S., Lin, Y., 2000. An estimation of turbulent kinetic energy and energy dissipation rate based on atmospheric boundary layer similarity theory, Virginia.

Hanna, S.R., Britter, R., Franzese, P., 2003. A baseline urban dispersion model evaluated with Salt Lake City and Los Angeles tracer data. Atmos Environ 37, 5069-5082.

Hill, T.A., Fackrell, J.E., Dubal, M.R., Stiff, S.M., 2011. Understanding the consequences of CO2 leakage downstream of the capture plant. Energy Procedia 4, 2230-2237.

HSE, 2005. List of approved workplace exposure limits (as consolidated with amendments October 2007) – EH 40/2005. HSE, Health and Safety Commission.

Hsieh, K.-J., Lien, F.-S., Yee, E., 2013. Dense gas dispersion modeling of CO2 released from carbon capture and storage infrastructure into a complex environment. International Journal of Greenhouse Gas Control 17, 127-139.

Koornneef, J., Spruijt, M., Molag, M., Ramírez, A., Turkenburg, W., Faaij, A., 2010. Quantitative risk assessment of CO2 transport by pipelines—A review of uncertainties and their impacts. J Hazard Mater 177, 12-27.

Kunz, O., Wagner, W., 2012. The GERG-2008 Wide-Range Equation of State for Natural Gases and Other Mixtures: An Expansion of GERG-2004. Journal of Chemical & Engineering Data 57, 3032-3091.

Lee, B.I., Kesler, M.G., 1975. A generalized thermodynamic correlation based on three-parameter corresponding states. AIChE Journal 21, 510-527.

Li, H., Jakobsen, J.P., Wilhelmsen, Ø., Yan, J., 2011. PVTxy properties of CO2 mixtures relevant for CO2 capture, transport and storage: Review of available experimental data and theoretical models. Applied Energy 88, 3567-3579.

Liu, X., Godbole, A., Lu, C., Michal, G., Venton, P., 2014. Source strength and dispersion of CO2 releases from high-pressure pipelines: CFD model using real gas equation of state. Applied Energy 126, 56-68.

Mahgerefteh, H., Atti, O., Denton, G., 2007. An Interpolation Technique for Rapid CFD Simulation of Turbulent Two-Phase Flows. Process Safety and Environmental Protection 85, 45-50.

Martynov, S., Brown, S., Mahgerefteh, H., Sundara, V., Chen, S., Zhang, Y., 2014. Modelling three-phase releases of carbon dioxide from high-pressure pipelines. Process Safety and Environmental Protection 92, 36-46.

Mazzoldi, A., Hill, T., Colls, J., 2009. A Consideration of the jet-mixing effect when modelling CO2 emissions from high pressure CO2 transportation facilities. Energy Procedia 1, 1571-1578.

Mazzoldi, A., Hill, T., Colls, J.J., 2008. CO2 transportation for carbon capture and storage: Sublimation of carbon dioxide from a dry ice bank. International Journal of Greenhouse Gas Control 2, 210-218.

Mazzoldi, A., Hill, T., Colls, J.J., 2011. Assessing the risk for CO2 transportation within CCS projects, CFD modelling. International Journal of Greenhouse Gas Control 5, 816-825.

Mazzoldi, A., Picard, D., Sriram, G., Oldenburg, C.M., 2012. Simulation-based estimates of safety distances for pipeline transportation of carbon dioxide. Greenhouse Gas Science and Technology 2, 1-18.

Metz, B., Davidson, O., Coninck, H.D., Loos, M., Meyer, L., 2005. IPCC special report on carbon dioxide capture and storage. Cambridge University Press, New York.

Molag, M., Dam, C., 2011. Modelling of accidental releases from a high pressure CO2 pipelines. Energy Procedia 4, 2301-2307.

Novembre, N., Podenzani, F., Colombo, E., 2006. Numerical study for accidental gas releases from high pressure pipelines, ECCOMAS CFD 2006, pp. 388-407.

Patel, N.C., Teja, A.S., 1982. A new cubic equation of state for fluids and fluid mixtures. Chem Eng Sci 37, 463-473.

Peng, D., Robinson, D.B., 1976. New 2-constant equation of state. Industrial & Engineering Chemistry Fundamentals 15, 59-64.

Peterson, E.W., Hennessey, J.P., 1978. On the Use of Power Laws for Estimates of Wind Power Potential. Journal of Applied Meteorology 17, 390-394.

Picard, D.J., Bishnoi, P.R., 1988. The importance of real-fluid behavior and nonisentropic effects in modeling decompression characteristics of pipeline fluids for application in ductile fracture propagation analysis. Can J Chem Eng 66, 3-12.

Pontiggia, M., Landucci, G., Busini, V., Derudi, M., Albac, M., Scaionic, M., Bonvicinid, S., Cozzanid, V., Rota, R., 2011. CFD model simulation of LPG dispersion in urban areas. Atmos Environ 45, 3913-3923.

Redlich, O., Kwong, J.N.S., 1949. On the thermodynamics of solutions. Chem Rev 44, 233-244.

Sand, I.Ø., Sjøen, K., Bakke, J.R., 1996. Modelling of release of gas from high-pressure pipelines. International Journal of Numerical Methods in Fluids 23, 953-983.

Scargiali, F., Grisafi, F., Busciglio, A., Brucato, A., 2011. Modeling and simulation of dense cloud dispersion in urban areas by means of computational fluid dynamics. J Hazard Mater 197, 285–293.

Seevam, P., Race, J., Downie, M., Barnett, J., Cooper, R., 2010. Capturing carbon dioxide: the feasibility of re-using existing pipeline infrastructure to transport anthropogenic CO2, The 8th International Pipeline Conference (IPC2010). ASME, Calgary, Alberta, Canada, pp. 129-142.

Soave, G., 1972. Equilibrium constants for modified Redlich-Kwong equation of state. Chem Eng Sci 27, 1196-1203.

Standards Australia, 2012. Pipelines - Gas and liquid petroleum, Part 1: Design and construction (AS 2885.1-2012), Sydney, Australia.

Sun, B., Utikar, R.P., Pareek, V.K., Guo, K., 2013. Computational fluid dynamics analysis of liquefied natural gas dispersion for risk assessment strategies. Journal of Loss Prevention in the Process Industries 26, 117-128.

Tauseef, S.M., Rashtchian, D., Abbasi, S.A., 2011. CFD-based simulation of dense gas dispersion in presence of obstacles. Journal of Loss Prevention in the Process Industries 24, 371-376.

van der Waals, J.D., 1873. Over de continuiteit van den gas – en vloestoftoestand. Leiden University., Netherland

Wagner, W., 2009. Description of the software package for the calculation of thermodynamic properties from the GERG-2004 XT08 wide-range equation of state for natural gases and other mixtures. RUHR-UNIVERSITÄT BOCHUM, Bochum.

Wareing, C.J., Fairweather, M., Falle, S.A.E.G., Woolley, R.M., 2014. Validation of a model of gas and dense phase CO2 jet releases for carbon capture and storage application. International Journal of Greenhouse Gas Control 20, 254-271.

Wen, J., Heidari, A., Xu, B., Jie, H., 2013. Dispersion of carbon dioxide from vertical vent and horizontal releases—A numerical study. Proceedings of the Institution of Mechanical Engineers, Part E: Journal of Process Mechanical Engineering 227, 125-139.

Whitbread, R., 2012. Carbon capture and storage: health and safety risks and regulation, Third International Forum on the Transportation of CO2 by Pipeline, Gateshead, UK.

Witlox, H.W.M., 2012a. Data review and Phast analysis (discharge and atmospheric dispersion) for BP DF1 CO2 experiments. DNV Software, London.

Witlox, H.W.M., 2012b. Data review and Phast analysis (discharge and atmospheric dispersion) for Shell CO2 experiments. DNV Software, London.

Witlox, H.W.M., 2014. Review of discharge data for CO2 pipe depressurisation experiments. DNV GL Software, London.

Witlox, H.W.M., Harper, M., Oke, A., 2009. Modelling of discharge and atmospheric dispersion for carbon dioxide releases. Journal of Loss Prevention in the Process Industries 22, 795-802.

Witlox, H.W.M., Harper, M., Oke, A., Stene, J., 2014. Phast validation of discharge and atmospheric dispersion for pressurised carbon dioxide releases. Journal of Loss Prevention in the Process Industries 30, 243-255.

Woolley, R.M., Fairweather, M., Wareing, C.J., Falle, S.A.E.G., Proust, C., Hebrard, J., Jamois, D., 2013. Experimental measurement and Reynolds-averaged Navier–Stokes modelling of the near-field structure of multi-phase CO2 jet releases. International Journal of Greenhouse Gas Control 18, 139-149.

Woolley, R.M., Fairweather, M., Wareing, C.J., Proust, C., Hebrard, J., Jamois, D., Narasimhamurthy, V.D., Storvik, I.E., Skjold, T., Falle, S.A.E.G., Brown, S., Mahgerefteh, H., Martynov, S., Gant, S.E., Tsangaris, D.M., Economou, I.G., Boulougouris, G.C., Diamantonis, N.I., 2014. An integrated, multi-scale modelling approach for the simulation of multiphase dispersion from accidental CO2 pipeline releases in realistic terrain. International Journal of Greenhouse Gas Control 27, 221-238.

Figure Captions:

Table Captions:

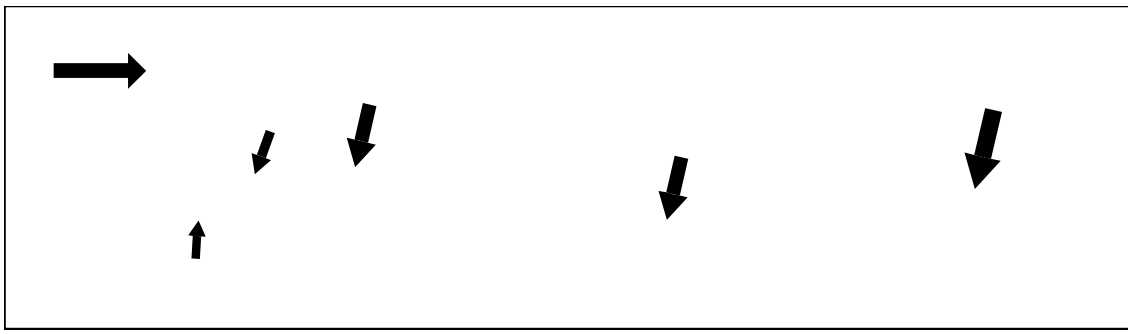

Fig. 1. CO_2 release from a high-pressure pipeline (Whitbread, 2012)

Fig. 2. Schematic of the problem partition (*P*: pressure, *T*: temperature, *u*: velocity; subscripts 0, *e* and *a* denote variables at stagnation conditions, at the exit plane, and at the atmospheric pressure plane respectively)

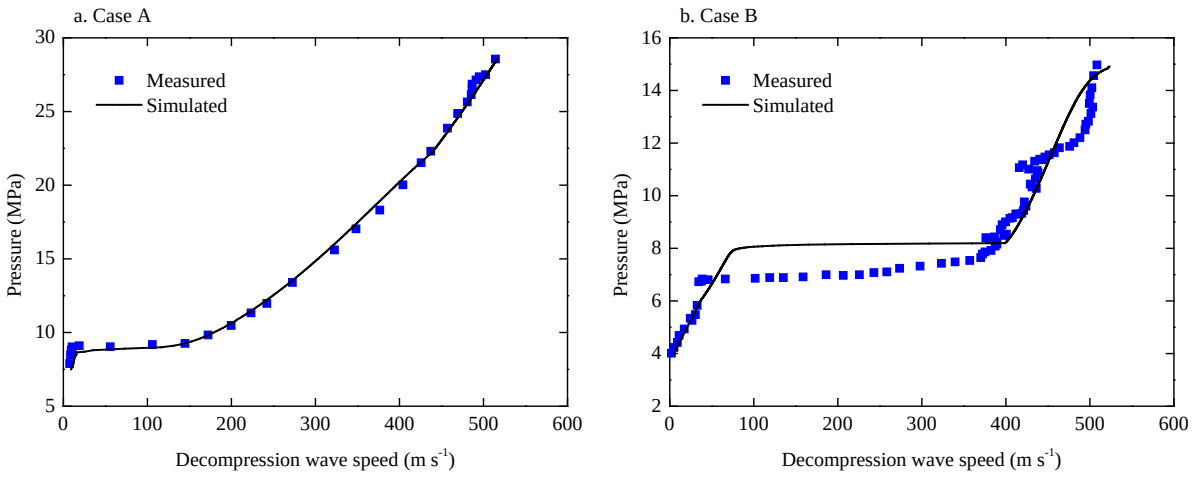

Fig. 3. Decompression wave speed - simulation vs measurement

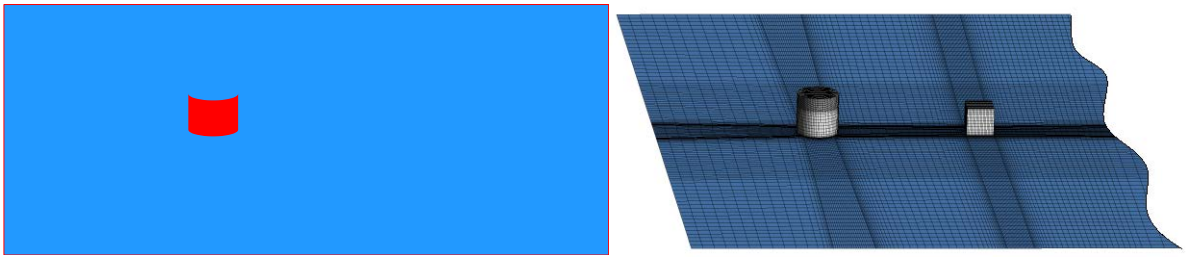

a. Schematic of Trial 26 b. Surface mesh

Fig. 4. Schematic of Thorney Island tests and the computational mesh

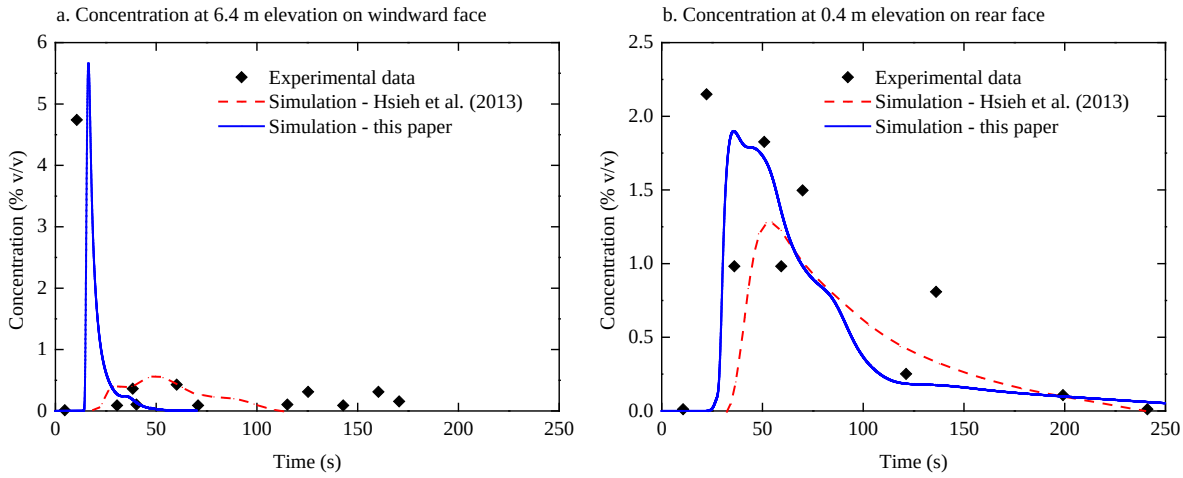

Fig. 5. Predicted gas concentration vs time of Thorney Island test Trial 26

Fig. 6. Full bore rupture simulation - computational mesh - schematic -

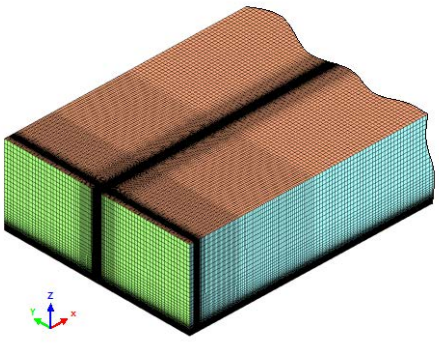

a. Computational domain b. Computational mesh

Fig. 7. Computational domain and mesh for the dispersion model

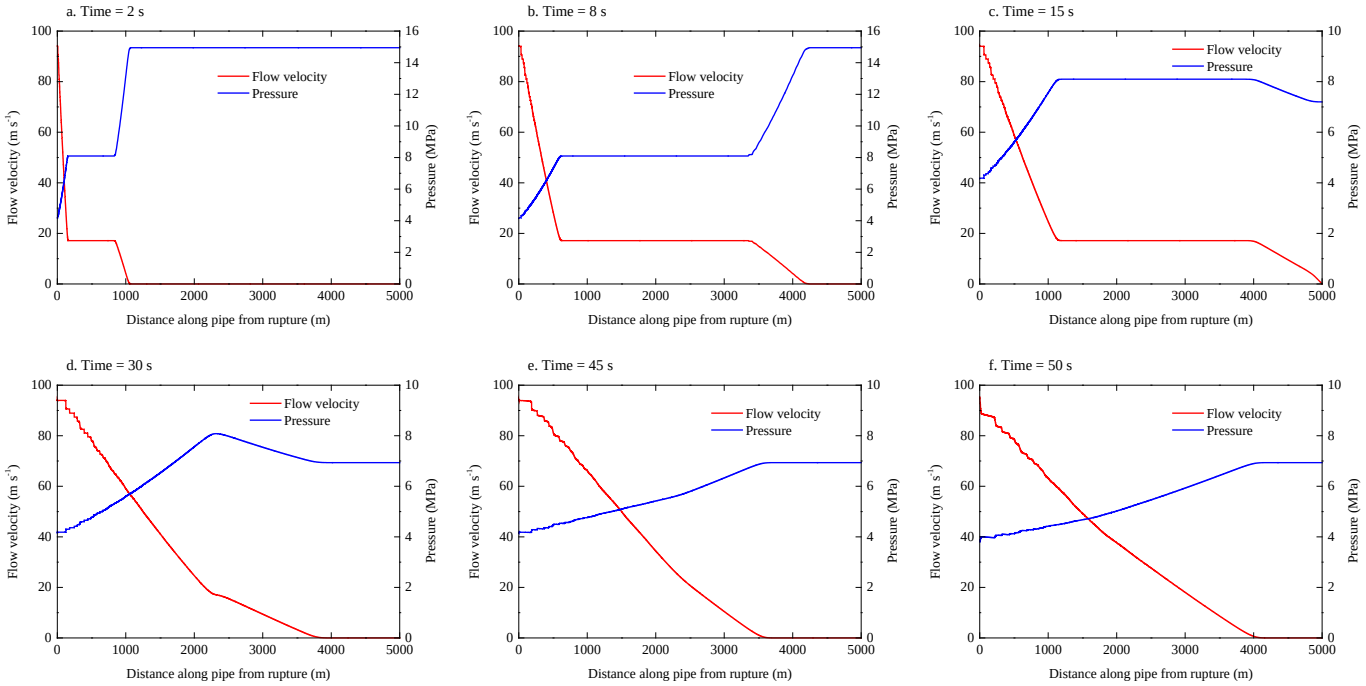

Fig. 8. Pressure and velocity profiles along the 5 km pipeline

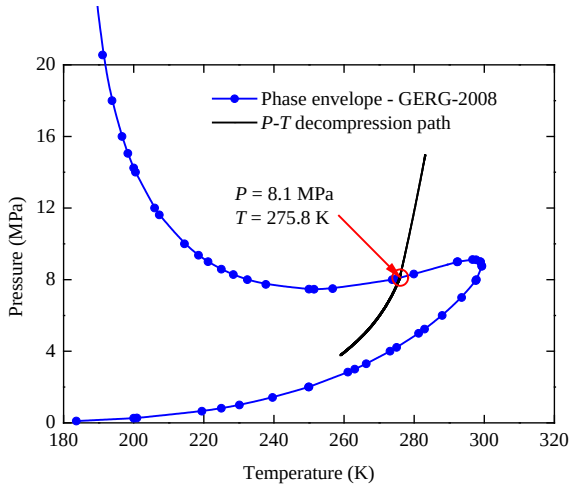

Fig. 9. Phase envelope of the mixture used in shock tube test case B and its decompression pressure-temperature curve

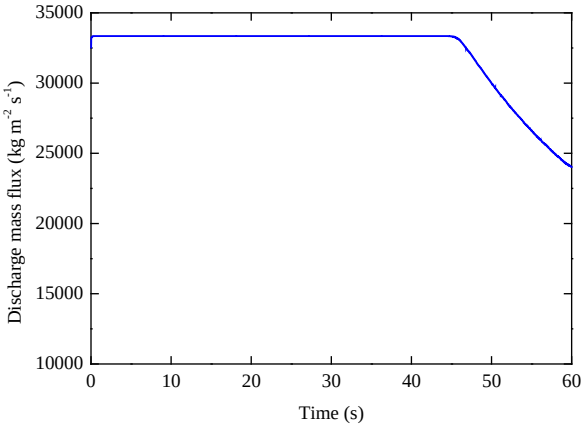

Fig. 10. Predicted mass flux at the rupture

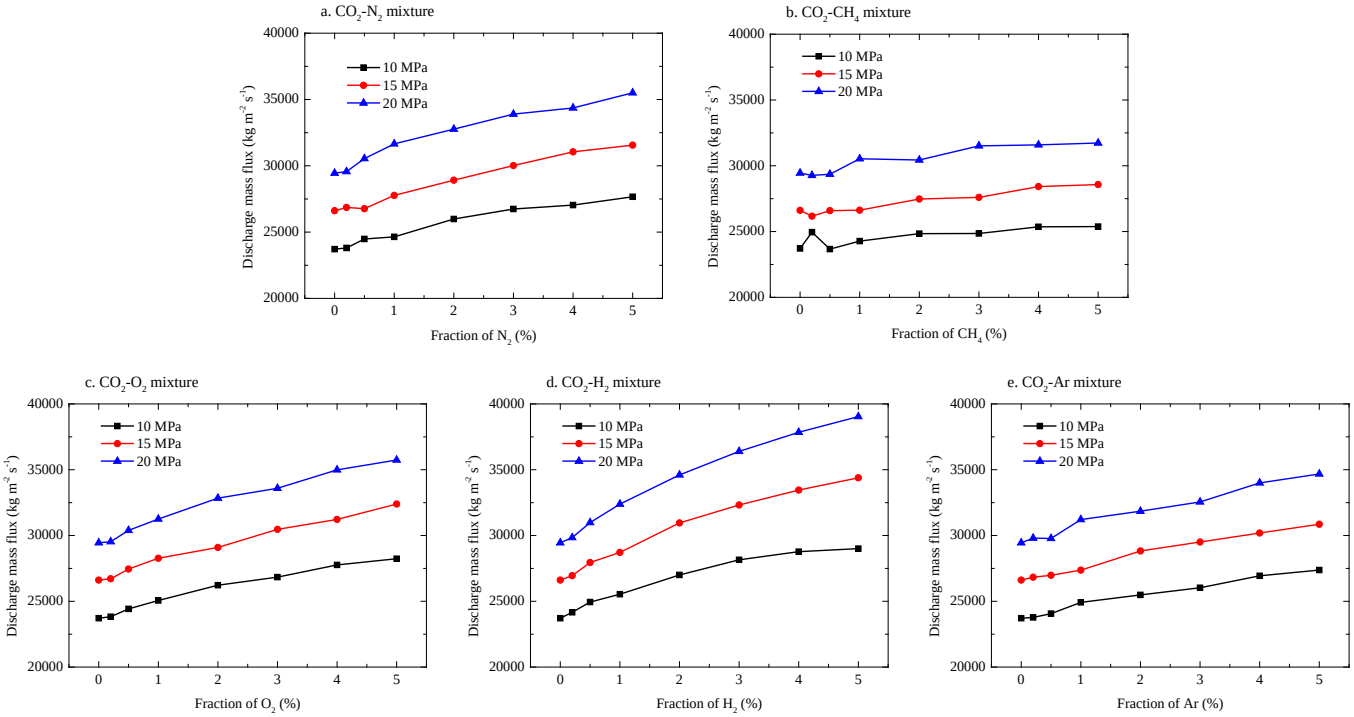

Fig. 11. Mass flux of a full-bore pipeline rupture for different binary CO_2 mixtures

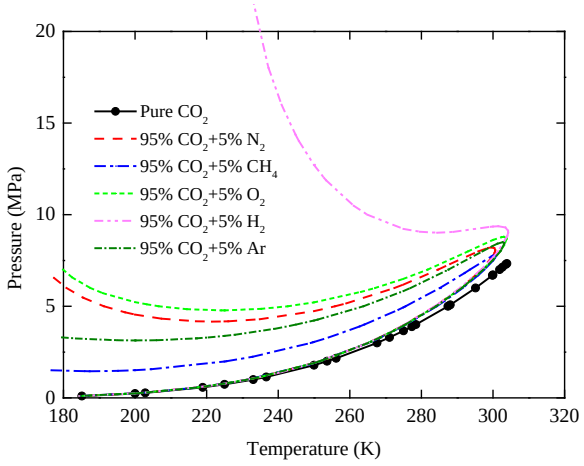

Fig. 12. Phase envelope of binary CO_2 mixtures calculated by GERG-2008 EOS

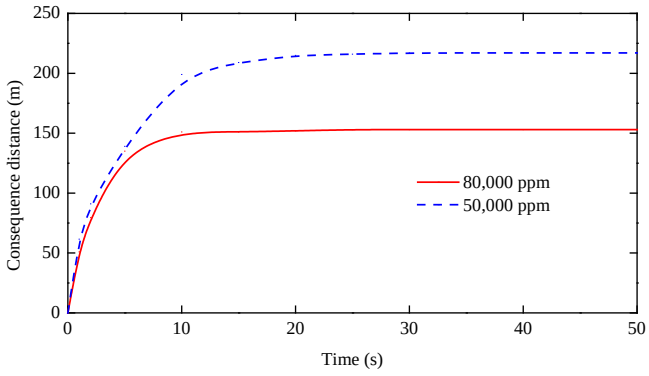

Fig. 13. Time history of consequence distance of hazardous cloud (ID = 400 mm, P_0 = 15 MPa, T_0 = 20 ºC)

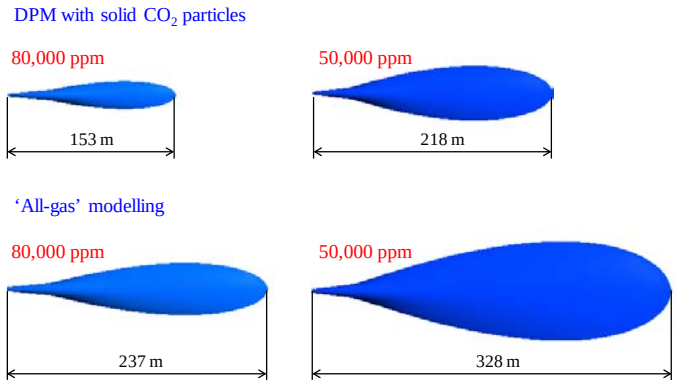

Fig. 14. Hazardous cloud – DPM vs 'all-gas' model (top view)

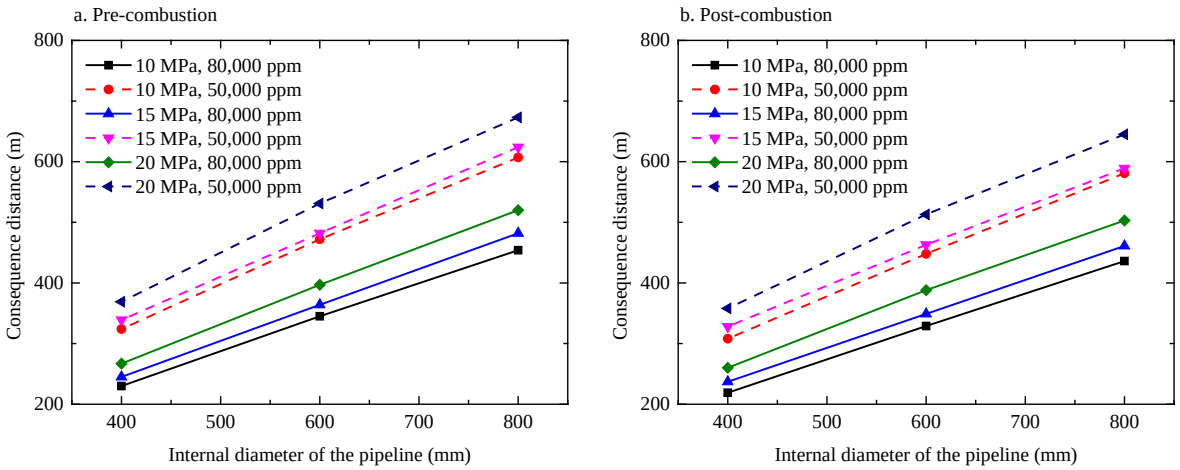

Fig. 15. Consequence distance for pre-combustion and post-combustion CO_2 mixtures

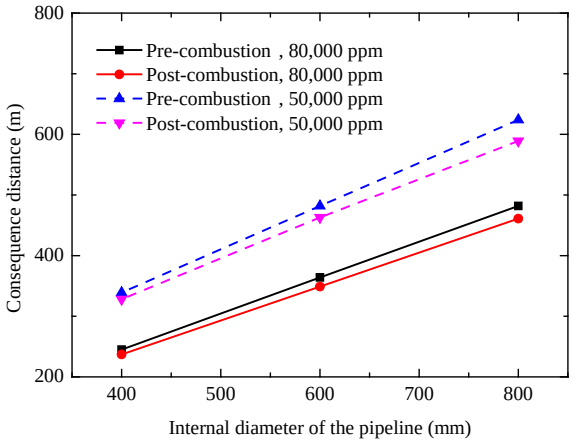

Fig. 16. Consequence distance – pre-combustion vs post-combustion (P_0 = 15 MPa)

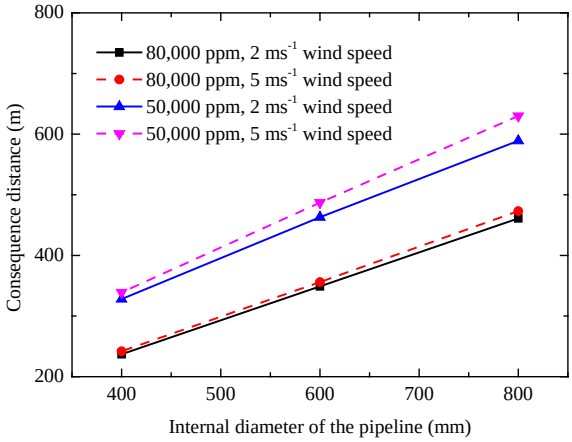

Fig. 17. Consequence distance for different wind speeds (post-combustion CO_2 mixture)

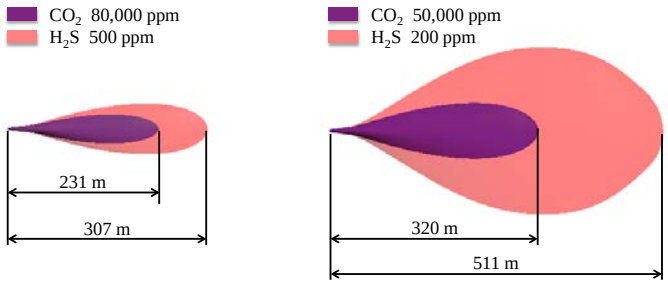

Fig. 18. Impact distances for CO_2 and H_2S (top view)

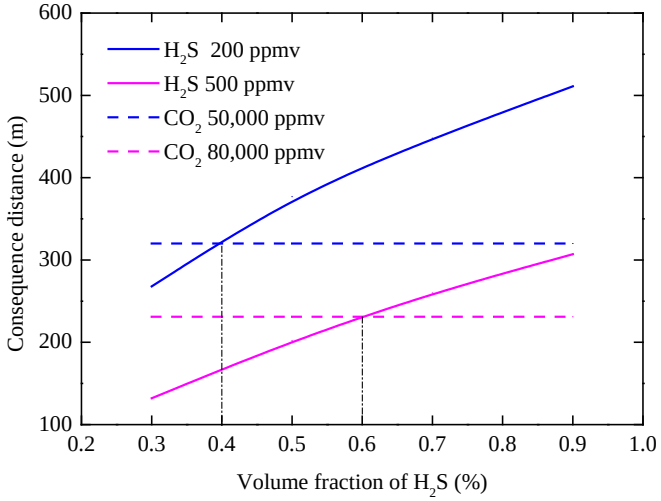

Fig. 19. Impact distances for CO_2 and H_2S for different H_2S fractions

Table 1 CO_2 mixtures - typical compositions for Australian conditions

Gas components	Post-combustion (mole %)	Pre-combustion (vol%)	Oxyfuel (vol%)
CO_2	99.97	95.66	95.87
N_2	0.01	0.43	1.38
O_2	0.01	0.43	1.38
CH_4		2	
H_2		1	
Ar	0.01	0.43	1.37
CO		0.04	
H_2S		0.01	

Table 2 Predicted discharge variables of typical CO_2 mixtures

CO_2 mixture	P_0 (MPa)	P_e (MPa)	T_e (K)	d_e (kg m^{-3})	u_e (m s^{-1})	Discharge mass flux (kg m^{-2} s^{-1})
Pre-combustion	10	3.5	266.6	280.2	96.7	27095
	15	3.8	267.4	354.3	86.1	30505
	20	4.0	268.4	434.5	78.9	34282
Post-combustion	10	3.0	267.9	286.5	83.9	24037
	15	3.2	269.3	397.8	66.8	26573
	20	3.5	273.4	525.8	57.7	30339
Oxyfuel	10	3.5	266.4	283.9	96.3	27340
	15	3.8	267.2	358.3	85.9	30778
	20	4.0	268.2	440.4	78.6	34615

Table 3 Flow variables at source plane for dispersion modelling

P_0 (MPa)	CO_2 mixture	Vapour mass fraction at exit (%)	Vapour mass fraction at source (%)	Source density (kg m^{-3})	Source velocity (m s^{-1})
10	Pre-combustion	24.4	48.9	5.66	223.0
	Post-combustion	23.2	48.9	5.66	209.7
15	Pre-combustion	18.0	46.2	5.99	206.0
	Post-combustion	14.4	45.0	6.15	183.8
20	Pre-combustion	13.4	44.5	6.22	193.4
	Post-combustion	9.5	44.5	6.21	172.8

Table 4 Health impact of CO_2 (Standards Australia, 2012)

Volume concentration (ppm)	Health effects
5,000	Long-term exposure limit in major jurisdictions
10,000	Slightly increased breathing rate
20,000	Doubled breathing rate, headache, tiredness
50,000	Very rapid breathing, confusion, vision impairment
80,000 – 100,000	Loss of consciousness after 5–10 minutes
> 100,000	More rapid loss of consciousness, death if not promptly rescued

Table 5 Health impact of Hydrogen Sulphide (Standards Australia, 2012)

Volume concentration (ppm)	Health effects
10 – 20	Long-term exposure limit in major jurisdictions; some eye irritation
100 – 200	Sense of smell lost (and hence warning of danger lost) Possible permanent eye damage
500	Loss of consciousness after a few minutes, significant possibility of death
1000	Immediate collapse and death after as little as a single inhalation